A test bed for verification of a methodology to correct the effects of range dependent errors on radar estimates

S. Sebastianelli[1], F. Russo[1], F. Napolitano[1], L. Baldini[2]

[1]*Dipartimento di Ingegneria Civile, Edile e Ambientale, Sapienza Università di Roma, via Eudossiana 18, 00184 Roma, Italia, stefano.sebastianelli@uniroma1.it*

[2]*Istituto di Scienze dell'Atmosfera e del Clima,Consiglio Nazionale delle Ricerche, via del Fosso del Cavaliere 100, 00100 Roma, Italia, l.baldini@artov.isac.cnr.it*

(Dated: 30 May 2012)

Dr. Luca Baldini (right) and Ing. Stefano Sebastianelli

1. Introduction

Quantitative radar precipitation estimates are affected by error determined by many causes that include, among others, radar miscalibration, range degradation (including beam broadening and sampling of precipitation at increasing altitude), attenuation, ground clutter, variability of *Z-R* relation, variability of drop size distribution, hydrometeor water phase distribution within the sampled volume, vertical variability of the precipitation system, vertical air motion, precipitation drift, anomalous propagation and beam-blocking (Zawadzki, 1984; Koistinen and Puhakka, 1986; Saltikoff et al., 2000; Villarini et al., 2008; Berenguer and Zawadzki, 2009; Villarini and Krajewski, 2010). Several sources, such as attenuation, range degradation and radar sampling above the clouds, determine a range dependent behaviour of error. The aim of this work is to quantify the range-dependent influence of the above-mentioned sources of uncertainties on rainfall radar estimates, through comparison between radar and rain gauge network precipitation fields. To reach this objective, the *G*/*R* ratio was calculated against range, where *G* and *R* are the corresponding rain gauge and radar rainfall amount, respectively, computed at each rain gauge location. Radar data are processed to compensate calibration and attenuation effects.

Finally, the range dependent error was modeled through an adjustment factor, derived for different elevation angles. Radar data were collected by the Polar 55C weather radar located in Rome (Italy) managed by the Institute of Atmospheric Sciences and Climate of the National Research Council (ISAC-CNR) of Italy in 2008. Rain gauges data were collected by the network of the Lazio regional administration located inside the radar scanning area. A subset of rain gauges appears as aligned along a given direction from the radar along a range of almost 120 km free from beam blocking effects is used to verify the effectiveness of the methodology. A set of five events is used to this purpose. This direction, which is almost parallel to the Tyrrhenian coast line, is also that along which intense convective cells tend often to organize themselves as a squall line. Such condition is verified in the considered dataset.

In the next section the data selection methodology is detailed. In Sect. 3 characteristics of Polar 55C weather radar are described, as well as the methodologies followed to calibrate weather radar with rain gauges, to perform radar rainfall estimates and to correct radar sampling errors and attenuation. In Sect. 4 logarithm of *G*/*R* trends with range, obtained before and after each processing of radar data, were compared, referring to different elevation angles. In Sect. 5 the influence of the melting layer on radar estimates is treated. Finally Sect. 6 completes the paper with conclusions.

2. Data

Polar 55C adopts different scanning strategies. The adopted strategies are based on the cyclical repetition of a certain number of PPI sweeps, each one with a constant elevation, ranging upward from two bounds. Elevation angles and scanning time are set according to the priorities of the ongoing research activity. Positive elevation angle allows satisfying the need to minimize the influence of ground-clutter and the contrasting need to keep the radar beam close to the ground (Gorgucci et al., 1995; Russo et al., 2005; Lombardo et al., 2006; Russo et al., 2006). This study considers measurements collected at antenna elevation angles ranging from 1.5 to 4.5°, because most of the used scanning strategies include these angles. The rainfall maps used in this study referred to the same elevation angle were acquired with a temporal resolution of 5 minutes.

To compute bias and adjustment factors, radar rainfall estimates are compared with the rain measured by a set of 40 rain gauges, managed by the Hydrographic and Oceanographic Office of the Lazio Regional Administration. Gauge rain is compared with radar estimates mapped onto 1 x 1 km^2 grid. Each pixel of the grid includes a number of radar beams that depends on the distance from radar. Rain gauges have time resolutions of 10 or 15 minutes and a rain resolution of 0.2 mm/h. Only rain gauges located in sectors with good radar visibility are considered, to avoid cases of partial or total beam-blocking. In particular, in order to verify the effectiveness of the methodology, only a subset of 17 rain gauges placed along a ray of the scanning circle was selected to make an optimal rain gauges network configuration for highlighting the effects of range dependent errors and attenuation. This ray corresponds to a direction almost parallel to the Tyrrhenian coast line along which several squall lines place themselves. Figure 1 shows the case-study region and the rain gauges positions respect to Polar 55C location. Five rainfall events observed during 2008 were considered in this study. Pairs of rainfall time series have been observed by Polar 55C and by each rain gauge at the rain gauge location during each of them. Moreover, to underline the effects of the signal attenuation, the events were chosen so that a squall line almost covers fully the path from

radar to the rain gauges, or this path is contained in a very intense rainy area during the whole of the considered event.

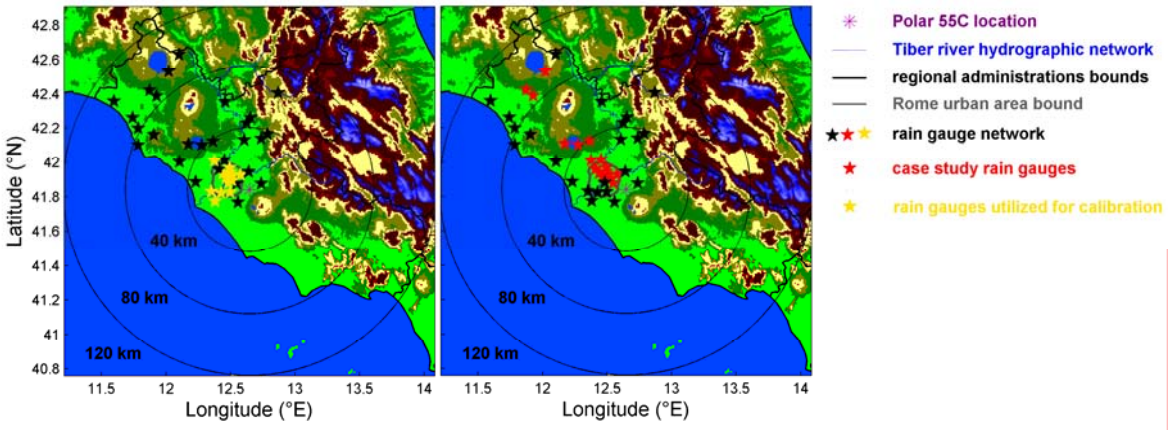

Fig. 1 - Rain gauge network inside Polar 55C scanning area. In yellow (left panel) and red (right panel) are the rain gauges selected for calibration and to verify the correction procedure, respectively.

3. Processing of radar data

Polar 55C is a C-band (5.6 GHz) Doppler dual polarized coherent weather radar with polarization agility managed by the ISAC-CNR in Italy. The radar is located 15 km South-East of Rome (lat. 41 °50'24" N, lon. 12°38'50" E, 102 m ASL). Radar measurements are obtained by averaging from 48 to 64 pulses transmitted with a 1200-Hz pulse repetition frequency in range-bin spaced apart of 75 m, up to 120 km away from the radar location (Gorgucci et al., 2002). Reflectivity data of Polar 55C are corrected for the calibration bias by adding a correction factor C to each recorded Z_h value. For this study, C is obtained from rain gauges calibration (Koistinen and Puhakka, 1986; Saltikoff et al., 2000). To calibrate Polar 55C the G/R ratio was computed by utilizing the dataset of radar and rain gauges collected in 2008. As suggested by Sebastianelli et al. (2012), rain gauges were selected so that radar errors in rain gauges sites were likely due only to radar miscalibration, to avoid the influence of the other kinds of errors on bias calculation.

The noise level is determined in each radar reflectivity map by supposing that, at great distance, the radar, also with relatively low elevations, samples with a good chance in an atmospheric region above the precipitation. In this way the modal value in the last two range-bins can be chosen as a reference to determine the noise level at the receiver that can be monitored in such a way during acquisitions. The noise estimated is a constant power and is converted into reflectivity in order to distinguish between signal and noise. The noise level at a range r can be expressed by Eq. (1) as follows:

$$Z_S(r) = Z_f + 20\log_{10}(r/r_{end}) \text{ dBZ} \quad (1)$$

where in the left-hand r_{end} is the maximum range and Z_f is the modal value determined as described before. Along each ray, Z_h values were compared at the range r with the Z_S values at the same ranges and the range-bins whose reflectivity does not exceed noise level by a threshold of 4 dB were considered affected by noise. Ground clutter removal is based on the existence of typical values for the standard deviations of the differential reflectivity $\sigma(Z_{DR})$ and of the differential phase $\sigma(\Phi_{DP})$ when the radar return is caused by precipitation (Bringi and Chandrasekar, 2001).

Only radar reflectivity which corresponds to meteorological returns was converted into rainfall intensity (R) by using a parametric algorithm, as (Gorgucci and Baldini, 2009):

$$R = 0.19055 \cdot 10^{\left(0.5358\left(Z_h/10\right)\right)} \text{ mm/h} \quad (2)$$

where Z_h is in dBZ. Coefficients of this algorithm are determined through simulations assuming theoretical derived distribution of the Drop Size Distribution (DSD) parameters, the drop shape model of Pruppacher and Beard (1970), a fixed temperature and the distribution of canting angle. Attenuation was corrected according to Testud et al. (2000).

Radar range error due to range degradation was corrected by adding an adjustment factor (AF), depending on the elevation angle, to each recorded Z_h value. The AFs were computed by utilizing rainfall events collected during 2008 by Polar 55C and 40 rain gauges placed in the radar scanning area (Sebastianelli et al. 2012). The G/R ratio between the rainfall amount at each gauge site (G) and the respective radar rainfall amount (R) was computed. A vector of G/R ratios was created, whose components are defined as follows:

$$\left(\frac{G}{R}\right)_j = \sum_{i=1}^{E} G_i \Big/ \sum_{i=1}^{E} R_i \quad j = 1, 2, \ldots, 40 \quad (2)$$

where G_i and R_i are the rain gauge and the radar rainfall amounts for the i-th event respectively, E is the number of rainfall events observed during 2008, and the subscript j refers to a specific rain gauge. Then the trend of the logarithm of G/R as a function of the range was evaluated for each elevation angle and two different behaviors were found depending both on the distance and on the elevation angle. Figure 2 shows an increasing linear trends of logarithm of the G/R ratios far from radar, represented by the best fitting lines. Vice versa, closer to the radar, the behavior of log(G/R) is influenced by the presence of the bright band, which causes a radar overestimation of rain, as better detailed in Sect. 5.

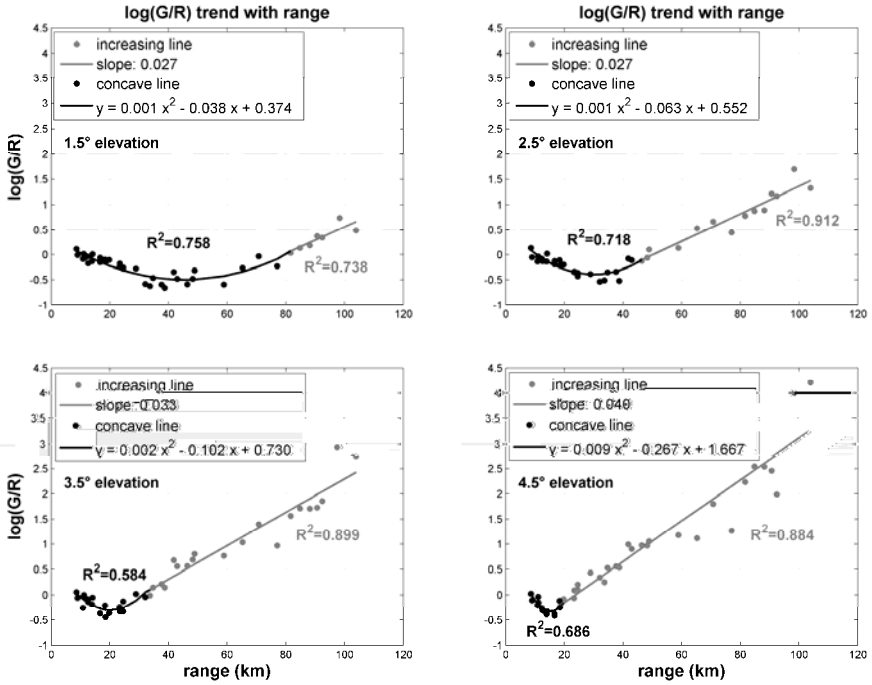

Fig. 2 Logarithm of the G/R ratios as a function of the range and best fitting lines. Each plot refers to a specific elevation angle.

The same procedure was followed for each elevation angle considered in this work, evaluating the *AF* trends showed in Fig. 3.

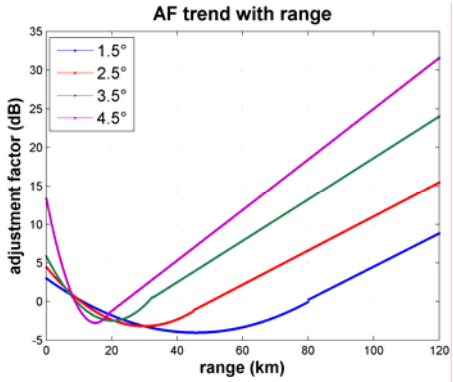

Fig. 3 - Trends of AF as a function of range from Polar 55C for each elevation angle.

The *AF* represents the overall radar error and it depends both on the distance and on the elevation angle. Therefore the *AF*s can be utilized to correct the reflectivity maps and consequently the radar rainfall estimates derived from radar reflectivity. Finally, radar rainfall intensity maps are obtained by remapping radar polar range-bins onto a 1 km^2 Cartesian grid.

4. Verification of the correction procedure

To verify the effectiveness of the methodology the subset of 17 rain gauges described in Sect. 2 was considered. The correspondence between pairs of rainfall processes observed, at the same time, by the radar and by each rain gauge at the rain gauge site was investigated through G/R ratio as a function of range from radar. Trends obtained before and after each processing of radar data were compared to show the improvement of radar estimates. For the present analysis only pairs of positive radar and rain gauge precipitation data were considered, since zero measurements decrease the spatial variability of data, by producing a high variability of the correlation between pairs of time series, with several abnormally high estimates

(Ha and Yoo, 2007). This comparison was made referring to the initial data set (without any correction) and repeated for different processing stages.

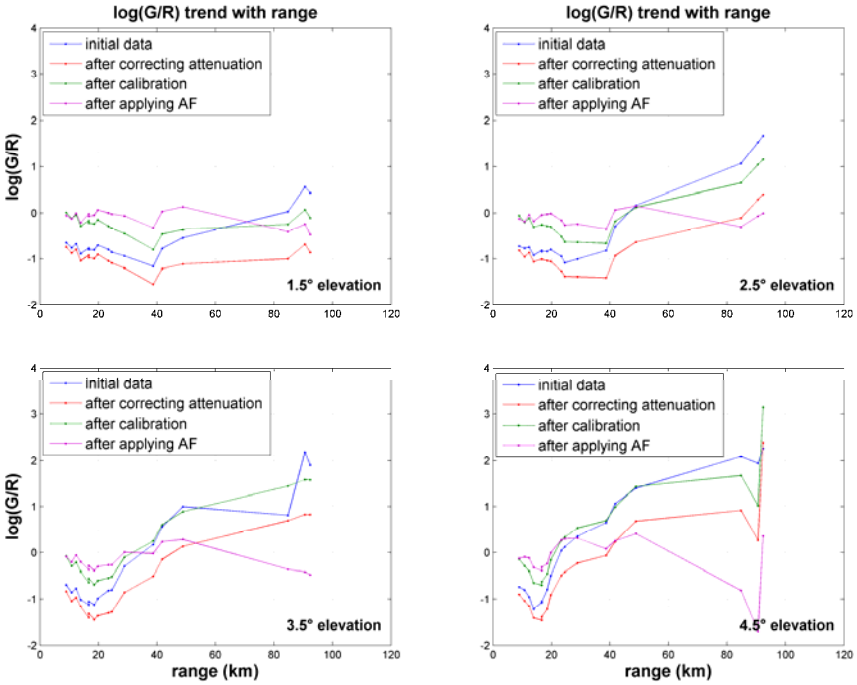

Fig. 4 G/R logarithm trends with range from Polar 55C evaluated for the initial radar data set, after signal attenuation correction, after radar calibration and after the adjustment procedure (blue, red, green and violet lines respectively); each plot is referred to a different elevation angle.

Before any correction, due to the negligible effects of range errors and to the presence of the melting layer, Polar 55C overestimates rainfall close to the radar, where log(*G*/*R*) has the lowest values. But, when the radar beam passes beyond the melting layer, sampling errors and attenuation effects become more important as the distance increases. Therefore, beyond a certain distance, depending on the elevation angle, log(*G*/*R*) values begin to increase up to a value of 0 or more. As a consequence, at first radar miscalibration effect is balanced and then Polar 55C underestimates rainfall especially close to the edge of the scanned area. Moreover, fixed the distance from radar, the greater is the elevation angle, the greater is the maximum value of log(*G*/*R*). After the attenuation correction the improvement of *G*/*R* (red curves in Fig. 4) is more evident at far ranges. A further improvement of radar estimates is obtained by calibrating radar. To perform radar calibration 40 rain gauges were utilized as explained in Sect. 2. Finally, after the adjustment procedure log(*G*/*R*) values are close to 0 all along the path, verifying the effectiveness of the followed methodology. But, at great distance from radar, it was not verified for the highest elevation angle, for which the number of homologues pairs with both intensity values different from zero, in corresponding pairs of rainfall processes, is so small that the curves are not meaningful.

5. Bright band

Curves in Fig. 5 represent log(*G*/*R*) trends against range obtained before any correction, at different elevation angles, by considering all the 40 rain gauges available for this study. As aforesaid, before any correction, because of the radar miscalibration, the negligible effects of range errors and the presence of the melting layer, Polar 55C overestimates rainfall close to its location, within a range of distances which depends on the elevation angle, as shown in Fig. 5. Correspondingly log(*G*/*R*) has the lowest values belonging to the first concave line of each curves. Instead, the second increasing line of each curve is due to attenuation and range degradation as above-mentioned. Moreover the slope of the second part of the curves increases as the antenna angle increases, because of the greater is the elevation angle, the greater is the effect of the range degradation. It must to be noted that the greater is the elevation angle: (1) the lower is the altitude at which the radar beam intercept the melting layer; (2) the shorter is the path needed to the radar beam to pass through the melting layer and (3) the bigger is the part of the radar sampling volume within the melting layer. As a consequence, as the elevation angle increases the length of the concave part become shorter and the minimum value decreases and moves to the origin of the coordinate system corresponding to radar site. This situation occurs during stratiform events, when the bright band signature is well defined. Instead, during convective events, bright band is not defined, because the intense updraft can stop the formation of a melting layer (Steiner et al., 1995) or there are different mixed phase altitudes depending on the considered storm cell. Therefore the trend of log(*G*/*R*) depends both on the location and on the number of storm cells, and there is no a concave part or an increasing part of the curve (not showed).

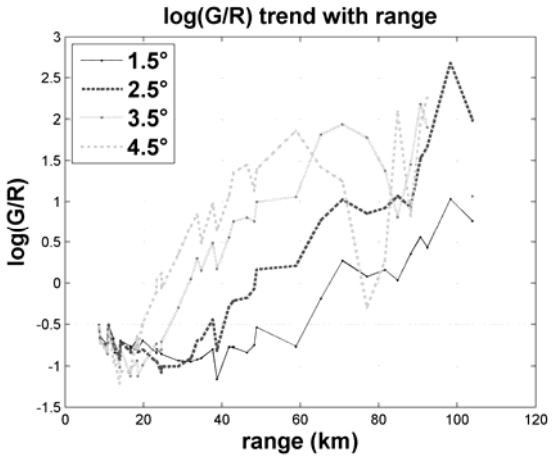

Fig. 5 – Trends of G/R logarithm as a function of range from Polar 55C evaluated for the initial radar data set considering all the 40 rain gauges available. Solid, dashed, dot, and dash-dot curves refer to 1.5, 2.5, 3.5 and 4.5° elevation angles respectively.

Since the *AF* is a function of the *G*/*R* ratio, the *AF* curves must have the same trend of log(*G*/*R*) curves. But the behavior of the minimum value in dependence of the antenna angle appears not so clearly as in Fig. 3, because the radar data set utilized includes both stratiform and convective events. Such consideration agrees with vertical profiles of reflectivity (VPR) simulations. The panel on the left of figure 6 shows a VPR observed from 75-m resolution vertical observation during the 15 December 2008 rainfall event, while the panel on the right shows the corresponding trends with distance from Polar 55C of log(*G*/*R*) obtained referring on different elevation angles ranging from 0.5 to 12°. To obtain trends shown in Fig. 6 (right), the VPR is considered as constant through all the ranges. Moreover, the same rainfall value was ascribed to the layers located in the vicinity of the ground, which was considered as the rain gauge value to calculate the *G*/*R* ratio.

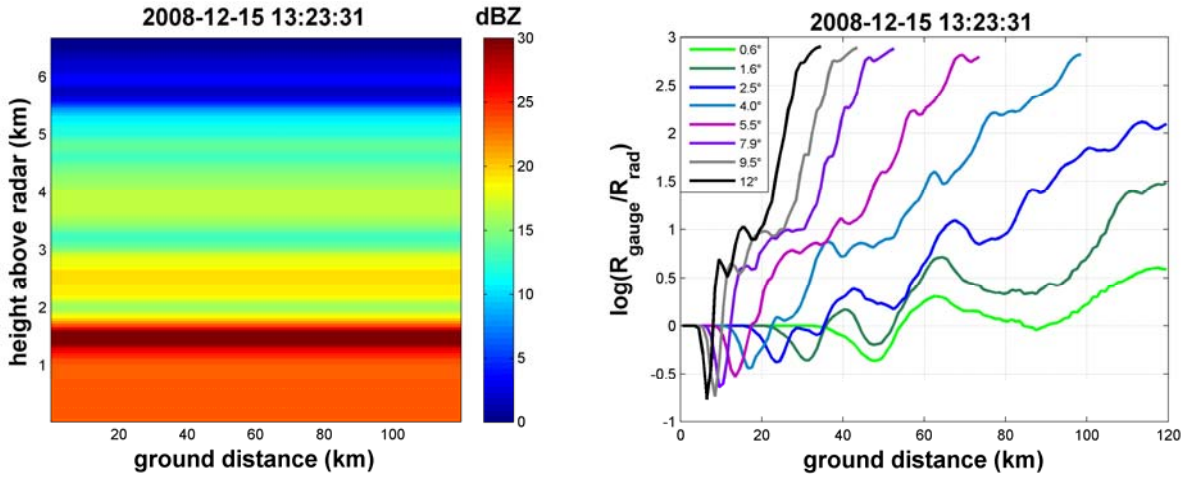

Fig. 6 VPR collected during the 15 December 2008 rainfall event and corresponding trends with distance from Polar 55C of log(G/R) obtained referring on different elevation angles ranging from 0.5 to 12°.

To demonstrate the influence of the melting layer on the profile of *AF* curves in dependence on the antenna angle, single rainfall events were considered. First log(*G*/*R*) curves were drawn for antenna angle ranging from 1.5 to 4.5° in Fig. 7. Left and middle panels in Fig. 7 refer to the 15 December 2008 rainfall event which is the case in point, whereas right panel refer to 7 March 2008 rainfall event and shows the same trends.

By observing the first concave part of the curves in Fig. 7, the maximum range from Polar 55C to which the melting layer influence the trend of *G*/*R* ratio could be obtained for each antenna elevation angle. Therefore, knowing the radar beam geometry it was possible to determine the maximum altitude of the melting layer, which was about 1950 m a.s.l.. At this point the nearby Pratica di Mare sounding site provided measurements of the 0° isotherm altitude throughout the considered event. Finally, for each elevation angle, the distance at ground at which the radar beam intercepts the mean 0° isotherm level (that is about 2030 m a.s.l.) was calculated and compared with the maximum distance at ground between Polar 55C site and the melting layer. The difference between the two distances ranges from 1 to 5 kilometer depending on the elevation angle, since the melting layer is always under the 0° isotherm level.

6. Conclusions

Many sources of errors that affect radar estimates determine a range dependent trend of the error between radar and rain gauge precipitation estimate. To investigate this issue the *G*/*R* ratio was calculated against range. By applying a method to

correct radar return for attenuation and after a calibration using nearby rain gauges, the range dependent errors trend against range was modeled through an adjustment factor.

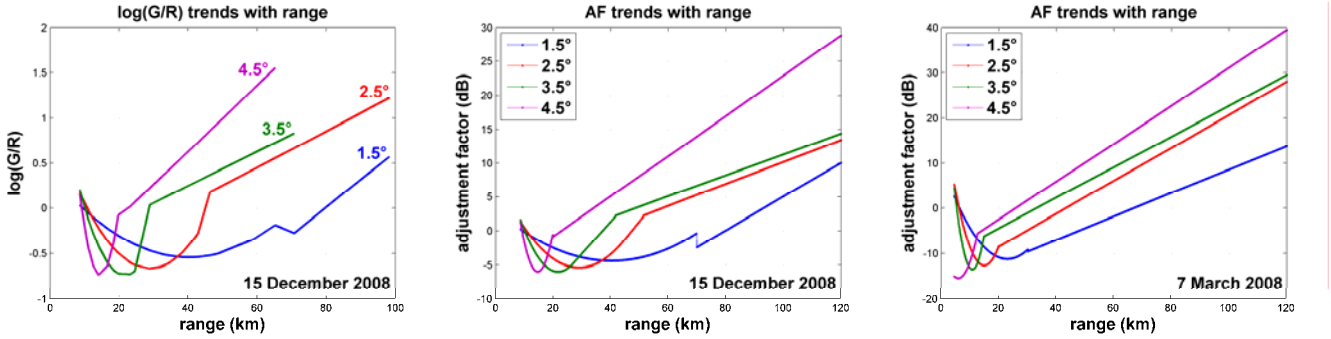

Fig. 7 log(G/R) and AF trends with range from radar for 15 December 2008 (left and middle panels respectively). The panel on the right shows trends of AF for 7 March 2008. Each plot considers 1.5, 2.5, 3.5, and 4.5° elevation angles.

The same procedure was performed referring to different elevation angles, to find how change the influence of the above-mentioned kind of errors. After the correction procedure, the *G*/*R* ratio, calculated by considering all the events observed in 2008, is close to one all along the path. Besides, four *AF* trends with range for Polar 55C were found, depending on the elevation angle. Each curve consists of two parts. The first one is concave and is due to the presence of the melting layer, and its shape depends on the considered elevation. The second one is an increasing function of the range and is due to the effect of the range degradation. The *AF* trend with range, referring to a specific elevation angle, can be used as a range error pattern, which allows to correct the mean error which affect radar estimates of rain (mm) provided during a long period of time. In fact, as showed above, there is not an univocal range error pattern, but it changes depending on the rainfall event. As a consequence the *AF* proposed is suitable for applications that require long-term precipitation estimates (mm), such as the quantitative estimation of precipitation necessary to evaluate the water budget of a basin.

References

Berenguer M., Zawadzki I., 2009: A study of the error covariance matrix of radar rainfall estimates in stratiform rain. Part II: scale dependence. *Weather Forecast.*, ***24***, 800– 811

Bringi V.N., Chandrasekar V., 2001: Polarimetric Doppler weather radar: principles and applications. *Cambridge University Press, New York, USA*

Gorgucci E., Baldini L., 2009: An examination of the validity of the mean raindrop-shape model for dual-polarization radar rainfall retrievals. *IEEE T. Geosci. Remote*, ***47(8)***, 2752– 2761

Gorgucci E., Baldini L., Volpi A., 2002: an upgraded instrument for polarimetric radar research. *Proceedings of the 2nd European Conference of Radar Meteorology ERAD Delft, The Netherlands, 18-23 November 2002*, 394– 399

Gorgucci E., Scarchilli G., Chandrasekar V., 1995: Radar and surface measurements of rainfall during CaPE. *J. Appl. Meteorol.*, ***34***, 1570– 1577

Ha E., Yoo C., 2007: Use of mixed bivariate distributions for deriving inter-station correlation coefficients of rainfall. *Hydrol. Process.*, ***21(22)***, 3078– 3086

Koistinen J., Puhakka T., 1986: Can we calibrate radar with raingauges. *Geophysica*, ***22 (1-2)***, 119– 129

Lombardo F., Napolitano F., Russo F., 2006: On the use of radar reflectivity for estimation of the areal reduction factor. *Nat. Hazard. Earth Sys.*, ***6***, 377– 386

Pruppacher R., Beard K.V., 1970: A wind tunnel investigation of the internal circulation and shape of water drops falling at terminal velocity in air. *Q. J. Roy. Meteor. Soc.*, ***96***, 247– 256

Russo F., Napolitano F., Gorgucci E., 2005: Rainfall monitoring systems over an urban area: the city of Rome. *Hydrol. Process.*, ***19(5)***, 1007– 1019

Russo F., Lombardo F., Napolitano F., Gorgucci E., 2006: Rainfall stochastic modelling for runoff forecasting. *Phys. Chem. Earth.*, ***31(18)***, 1252– 1261

Sebastianelli S., Russo F., Napolitano F., Baldini L., 2012: On precipitation measurements collected by a weather radar and a rain gauge network. *Nat. Hazard. Earth Sys.*, ***in review***

Saltikoff E., Koistinen J., Hohti H., 2000: Experience of real time spatial adjustment of the Z-R relation according to water phase of hydrometeors. *Phys. Chem. Earth*, ***25***, 1017– 1020

Steiner M., Houze J.R.A., Yuter S.E., 1995: Climatological characterization of three-dimensional storm structure from operational radar and rain gauge data. *J. Appl. Meteorol.*, ***34***, 1978– 2007

Testud J., Le Bouar E., Obligis E., Ali-Mehenni M., 2000: The rain profiling algorithm applied to polarimetric weather radar. *Journal of atmosphericand oceanic technology*, ***17***, 332– 356

Villarini G., Serinaldi F., Krajewski W.F., 2008: Modeling radar-rainfall estimation uncertainties using parametric and non-parametric approaches. *Adv. Water Resour.*, ***31***, 1674– 1686

Villarini G., Krajewski W.F., 2010: Review of the different sources of uncertainty in single polarization radar-based estimates of rainfall. *Surv. Geophys.*, ***31 (1)***, 107– 129

Zawadzki I., 1984: Factors affecting the precision of radar measurements of rain. *Proceeding of the 22d Conf. Radar Meteorology, Zurich, Switzerland, 10-13 September 1984*, ***Amer. Meteor. Soc.***, 251– 256